A method of extending the capabilities of multispectral interference-filter cameras for planetary exploration and similar applications

Gunn, Matthew David; Barnes, Dave; Cousins, Claire R.; Langstaff, David Philip; Tyler, Laurence Gethyn; Pugh, Stephen Medwyn; Pullan, Derek; Griffiths, Andrew D.

Publication date:
2011

Citation for published version (APA):
Gunn, M. D., Barnes, D., Cousins, C. R., Langstaff, D. P., Tyler, L. G., Pugh, S. M., Pullan, D., & Griffiths, A. D. (2011). *A method of extending the capabilities of multispectral interference-filter cameras for planetary exploration and similar applications*. 108-113. Paper presented at Proceedings of University of Strathclyde's Second Annual Academic Hyperspectral Imaging Conference, Strathclyde, United Kingdom of Great Britain and Northern Ireland. http://www.strath.ac.uk/media/departments/eee/cesip/hsi/proceedings-of-hsi_2011.pdf

A method of extending the capabilities of multispectral interference-filter cameras

for planetary exploration and similar applications

Matthew Gunn[1], Dave Barnes[1], Claire R Cousins[2], Dave Langstaff[1], Laurence Tyler[1], Stephen Pugh[1], Derek Pullan[3], Andrew D. Griffiths[4]

[1]Aberystwyth University*, SY23 3BZ, UK
[2]Centre for Planetary Sciences, University College London, WC1E 6BT, UK
[3]Department of Physics and Astronomy, University of Leicester, LE1 7RH, UK
[4]MSSL, University College London, RH5 6NT, UK

The capabilities and benefits of hyperspectral imaging in remote sensing applications are well established and routinely exploited in terrestrial imaging applications. However the restrictions imposed on mass and power consumption and the extreme operating conditions encountered on other planets have limited its widespread use in planetary exploration robots. Instead multispectral camera systems using a small number of optical filters (typically 10-12) are employed, providing only coarse spectral information. By exploiting the properties of interference filters at non normal angles of incidence it is possible to obtain additional spectral information using established multispectral filter wheel camera technology. This additional information can help in identification of mineralogical species present by inferring the existence of spectral features missed between filter wavelengths. Examples of the implementation and capabilities are presented using simulated data for the PanCam instrument under development for the ESA / NASA ExoMars 2018 mission. By extension of the technique and with recent advances in interference filter technology it is possible to develop a simple and lightweight hyperspectral wide angle camera employing a filter wheel. The theory of operation and early test results from a prototype camera system are presented.

Key Words: interference filter, tunable filter, filter wheel, PanCam, multispectral

I. INTRODUCTION

Many methods are used in exploring the surface of other planets but a particularly powerful and versatile remote sensing technique is multispectral imaging. By combining optical spectroscopy and digital imaging, multispectral and hyperspectral imaging provide a means of enhancing subtle contrasts and remotely identifying and characterizing materials and minerals by their spectral signatures. A key application of the multispectral imaging instruments on previous planetary exploration rovers is mapping the geology in proximity to the rover as a means of identifying potential science targets. This will be equally true of the ESA / NASA ExoMars 2018 mission, the main aim of which is the search for traces of past or present life [1]. The suite of instruments which make up the Pasteur payload on ExoMars provides numerous analytical methods of identifying and analyzing samples obtained on and below the Martian surface but in order to use the majority of these instruments a sample must first be collected. The inclusion of a drill to obtain sub surface samples provides a unique capability to ExoMars but the risk involved in deploying it means that there has to be a high degree of certainty that it will be drilling in the right place.

On the ExoMars mission the task of surveying the Martian surface to find suitable science targets will fall largely to the mast mounted panoramic camera system – PanCam [2]. This consists of a pair of filter wheel based multispectral wide angle cameras (WACs) separated by 0.5m and a narrow field of view high resolution camera (HRC) mounted on a single optical bench. The WACs have a total of 22 filters distributed between them - 3 broadband RGB filters each for color Digital Elevation Model (DEM) reconstruction, 12 narrowband geology filters and 4 filters for atmospheric studies. The optical bench is mounted at a height of 1.8m on a pan tilt unit at the top of the rover mast, providing a high vantage point and allowing the cameras to be pointed in almost any direction. By combining high resolution stereo imaging, DEM generation and multispectral imaging it is designed to identify regions of scientific interest most likely to harbor traces of life. Key to this task will be the identification of lithologies containing hydrated minerals, which are high priority targets due to their association with past liquid water [3]. Such lithologies will be remotely classified and interpreted based on their multispectral properties captured by PanCam using the geology filter set.

In the spectral range covered by the PanCam and previous instruments (440 - 1000 nm) there are few distinctive spectral features to aid in mineral identification. Reflectance spectra measured by PanCam will consist of only 12 well separated spectral points and so it will be easy to miss diagnostic spectral features. Unfortunately the strict limitations on mass, power and data return bandwidth prohibit the use of a larger set of geology filters. Alternative spectral imaging hardware is available such as Acousto-Optic Tunable Filters (AOTF) and Liquid Crystal Tunable Filters (LCTF) which can provide wide and continuous wavelength tuning ranges. However, mass, complexity and their increased power consumption currently make them unsuitable for use in extraterrestrial environments.

Although every effort is being made to ensure that the 12 geology filters in PanCam will allow detection of as many diagnostic spectral features as possible, it will not be possible

* Corresponding Author: Matt Gunn, email mmg@aber.ac.uk

to cover them all. However, by exploiting the properties of interference filters off axis it should be possible to obtain additional spectral information not only with ExoMars PanCam but also with existing multispectral filter wheel cameras.

II. METHOD

A. *Off axis properties of interference filters*

Thin film filters such as those employed in multispectral filter wheel cameras work on the principle of optical interference – constructive interference ensures a high transmission in the pass band and destructive interference provides a high optical density outside the pass band. Filters consist of a stack of thin optical coatings on a transparent substrate and the optical path lengths through the films are optimized to obtain the required interference. In addition to the thickness and refractive index of the films, the optical path length is also dependent on the angle of incidence of the light – the angle of the incident rays with respect to the filter surface normal. As the optical path lengths in the films are affected by the angle of incidence, the transmission characteristics of the filter are also affected resulting in a shift of the pass band to shorter wavelengths as the angle of incidence is increased. This characteristic of interference filters is exploited for fine tuning the transmission edge of filters in applications such as Raman spectroscopy where it is used for blocking only the Rayleigh scattered light. The shifted centre wavelength (λ) for a given angle of incidence (θ) is related to the wavelength at normal incidence (λ_0) and the effective refractive index of the thin film stack (n_{eff}) by [4]:

$$\lambda = \lambda_0 \cdot \sqrt{1 - \frac{\sin^2(\theta)}{n_{eff}^2}} \,. \qquad (1)$$

As can be seen from (1), for a given angle of incidence, the shift obtainable is dependent on the effective refractive index of the thin film stack which is determined by the material properties and the stack structure. In order to determine typical values for the effective refractive index, filters in the flight spare filter wheel from the Beagle 2 panoramic camera [5] were analyzed. A collimated beam of white light was passed through each filter and the transmitted spectrum measured with an Ocean Optics Jaz spectrometer. The filter wheel was mounted on a rotation stage so that the angle of incidence could be manually adjusted. Measurements were taken at 1° increments in the angle of incidence and the percentage transmission was obtained by normalizing the measured spectra to the incident white light spectrum. Spectra for the 600nm filter at several angles are presented in Fig 1.

The centre wavelengths, full width at half maximum and maximum transmission were determined by fitting a Gaussian function to each measured transmission spectrum with a Levenberg-Marquadt algorithm in Mathcad. Equation (1) was then fitted to the peak positions using the same fitting algorithm. The measured and fitted wavelength shifts as a function of angle of incidence are shown in Fig 2 along with the variation of maximum transmission.

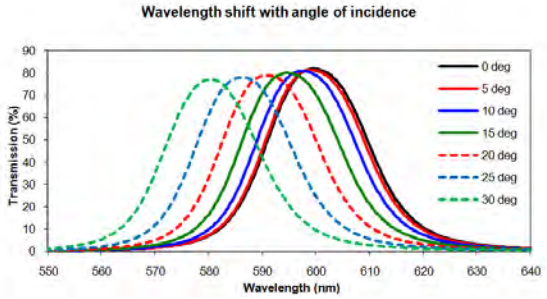

Figure 1. Transmission profiles of Beagle 2 600nm filter over a range of angles of incidence.

The fitting gave the effective refractive index for the 600nm filter shown in Fig 1 as 1.98 and values for the other filters in the wheel ranged from 1.94 to 2.31 with most lying between 1.98 and 2.15.

B. *Implications for filter wheel cameras*

With an endocentric lens (one in which the entrance pupil is at a finite distance) the angle of incidence of the light passing through the filter will vary across the field of view. For a rectilinear lens (one which produces little or no distortion) the angle of incidence of the rays passing through the filter is directly proportional to the image height. With a lens which is both endocentric and rectilinear such as the one shown in Fig 3 the wavelength of the light reaching the detector is therefore proportional to the image height.

For a given filter the range of the wavelength shift depends on the range of angles of incidence and hence on the field of view of the camera. In the case of PanCam the field of view horizontally (and vertically) will be 34° and diagonally 48°. The maximum angles of incidence will therefore be 17° and 24° respectively. It can be seen from Fig 2 that shifts of around 1% and 2% of the centre wavelength will be obtained at the edges and corners of the field of view respectively (assuming the filters to be similar to those used for Beagle 2). In the case of the MER cameras [6] the field of view horizontally (and vertically) was 16° and diagonally 22.5°. The maximum angle of incidence was therefore 11.25° (diagonally) and so maximum shifts of around 0.5% of the centre wavelength would be obtained.

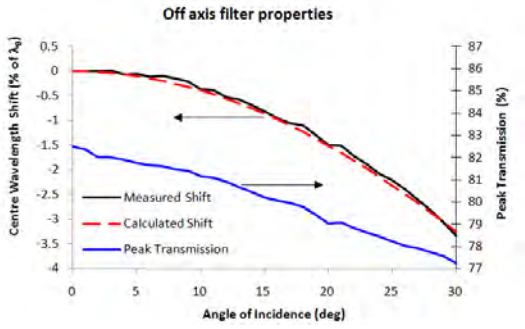

Figure 2. Beagle 2 600nm filter centre wavelength shift and peak transmission as a function of angle of incidence.

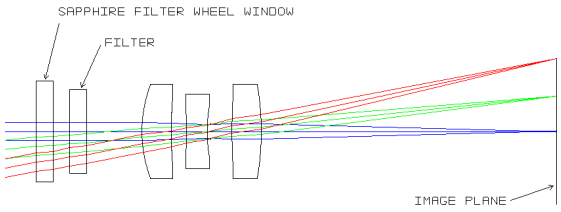

Figure 3. MER PanCam lens showing off axis ray bundles passing through filter at non zero angles of incidence. Lens prescription data from [7].

The geology filter selections for different missions vary but on average the filters are spaced at roughly 50nm intervals over the range 440 - 1000nm and the filter bandwidths (full width at half maximum - FWHM) vary between 15 - 42nm. For PanCam the spectral shifts at the edge of the field of view are likely to be between 4 - 10nm (depending on the filter wavelength) and for MER they are likely to be around half this. It can be seen that these shifts are small in comparison to the spacing between the filters and so the effect on the generated spectra is not likely to be too significant.

C. Exploiting the wavelength shift

As explained above there will always be a variation in the wavelength across the field of view of the camera. It is therefore possible to obtain spectral information centered at more than one wavelength with a single filter by taking two or more images and panning or tilting the camera between them. From the results presented in sections A and B it is evident that although there will be a difference in the wavelength at which an object of interest is imaged, the shift will be too small in comparison to the spacing between the geology filters to effectively fill the gaps.

A common method of filling the gaps between measured data points is by fitting a cubic spline through the data and using this to interpolate additional data points. Fitting a cubic spline involves calculating the coefficients (a, b, c, d) so that a cubic equation of the form:

$$y = a \cdot x^3 + b \cdot x^2 + c \cdot x + d \tag{2}$$

passes through a pair of consecutive measured data points (x_n, y_n), (x_{n+1}, y_{n+1}) where the subscript n represents the n^{th} data point (or the filter used to measure it). As there are four unknown coefficients it is necessary to obtain four boundary conditions to obtain a unique solution. Two of these boundary conditions are the measured coordinates of the two end points of the spline section. The other two conditions are generally obtained by ensuring that the gradients of the spline section on either side of each measured data point match. Although such a cubic spline will give a continuous and smooth line passing through all of the data points, there is insufficient information to ensure an accurate fit. Assumptions must be made about the gradients at the end points of the spline and it will not necessarily follow the original system from which the data points were obtained. This is shown for the case of an arbitrary function in Fig 4.

In order to effectively exploit the small variation in wavelength across the field of view it is possible to use pairs of closely spaced data points measured with a single filter to determine the gradient of the reflectance spectrum at that filters wavelength. This additional information can then be used to accurately fit a cubic spline through the data and thus allow accurate interpolation of additional data points. The gradient of the measured reflectance spectrum at the wavelength of the n^{th} filter (R'_n) is obtained as:

$$R'_n = \frac{R_{n,c} - R_{n,e}}{\Delta\lambda_n} \tag{3}$$

where $R_{n,c}$ and $R_{n,e}$ are the reflectances measured with the n^{th} filter for the object at the center and edge of the field of view respectively and $\Delta\lambda_n$ is the wavelength shift between the centre and edge of the field of view. The gradient of the cubic spline is obtained by differentiating (2) to obtain:

$$y' = \frac{dy}{dx} = 3 \cdot a \cdot x^2 + 2 \cdot b \cdot x + c\,. \tag{4}$$

A spline section links each pair of data points and coefficients must be found for each spline section. If there are N data points in the data set then there will be N-1 spline sections and sets of coefficients. The coefficients for the n^{th} spline section are found by substituting coordinates for a pair of measured data points and the gradient at each point – (λ_n, R_n, R'_n), (λ_{n+1}, R_{n+1}, R'_{n+1}) – into (2) and (4) to obtain four equations with four unknowns:

$$\begin{aligned} R_n &= a_n \cdot \lambda_n^{\,3} + b_n \cdot \lambda_n^{\,2} + c_n \cdot \lambda_n + d_n \\ R'_n &= 3 \cdot a_n \cdot \lambda_n^{\,2} + 2 \cdot b_n \cdot \lambda_n + c_n \\ R_{n+1} &= a_n \cdot \lambda_{n+1}^{\,3} + b_n \cdot \lambda_{n+1}^{\,2} + c_n \cdot \lambda_{n+1} + d_n \\ R'_{n+1} &= 3 \cdot a_n \cdot \lambda_{n+1}^{\,2} + 2 \cdot b_n \cdot \lambda_{n+1} + c_n \end{aligned} \tag{5}$$

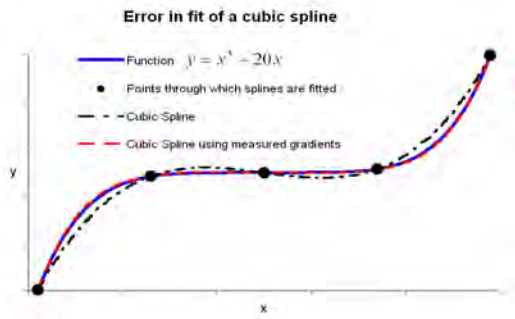

Figure 4. Plot showing a cubic spline passing through a set of data points but not accurately representing the original function. Also shown is a cubic spline calculated using gradients which accurately re-creates the original function.

Equations (5) must be solved simultaneously to obtain the coefficients. This can be achieved by expressing them in matrix form:

$$M_n \cdot \begin{pmatrix} a_n \\ b_n \\ c_n \\ d_n \end{pmatrix} = \begin{pmatrix} R_n \\ R_{n+1} \\ R'_n \\ R'_{n+1} \end{pmatrix} \tag{6}$$

where $$M_n = \begin{pmatrix} \lambda_n^{\,3} & \lambda_n^{\,2} & \lambda_n & 1 \\ \lambda_{n+1}^{\,3} & \lambda_{n+1}^{\,2} & \lambda_{n+1} & 1 \\ 3\cdot\lambda_n^{\,2} & 2\cdot\lambda_n & 1 & 0 \\ 3\cdot\lambda_{n+1}^{\,2} & 2\cdot\lambda_{n+1} & 1 & 0 \end{pmatrix}. \tag{7}$$

The coefficients for each spline are then obtained by substituting the inverse of matrix (7) into both sides of (6) to obtain:

$$\begin{pmatrix} a_n \\ b_n \\ c_n \\ d_n \end{pmatrix} = M_n^{\,-1} \cdot \begin{pmatrix} R_n \\ R_{n+1} \\ R'_n \\ R'_{n+1} \end{pmatrix}. \tag{8}$$

which may be conveniently solved by computer. The complete spline through all the data points is then pieced together from the N-1 spline sections by substituting the coefficients for each section into (2).

In practice it is envisaged that a sequence of images would be captured using the full set of geology filters as normal. If an unusual or particularly interesting feature is identified in the images then an additional sequence (or sequences) of images could be captured to obtain the maximum amount of spectral information. This could then be used to fit a cubic spline as outlined above. Although additional power would be required to carry out this operation in order to move the pan tilt unit and operate the filter wheel and cameras, it is not believed that this would be a limiting factor. The bandwidth required to transmit the additional images could be a limiting factor but it is only necessary to transmit the regions of interest. A full set of 24 sub images could be transmitted with less bandwidth than a single full image depending on the size of the region of interest. The Automatic Pointing and Image Capture (APIC) software [8] developed for ExoMars incorporates all the algorithms required to point the cameras at an object of interest and to extract the region of interest from the full images.

III. RESULTS

The ExoMars PanCam which has been the basis for much of the work feeding into this study is at an advanced stage of development but a fully functioning prototype is not yet available to test this technique. Instead simulations have been carried out using the F2-12 [3] filter set proposed for PanCam in combination with reflectance measurements taken on Mars analogue samples from Iceland. We note that the geology filter set for the ExoMars PanCam are still under development [9], and the F2-12 filter set, whilst not the final filter wavelengths, represent the most up-to-date published iteration of this development. A wavelength shift of 1% of each filter centre wavelength was assumed for the simulations and the centre and shifted wavelengths of the F2-12 filter set are presented in Table 1. Filters have been simulated as having a Gaussian transmission profile which was found to be a reasonable approximation for the filters in the Beagle 2 filter set. A bandwidth (FWHM) of 15nm was used for all filters.

Both Mars analogue samples are acid-weathered basaltic lavas with mineralogical deposits in the lava vesicles. Distinctive colored regions are attributed to the sulfur-rich alteration products. Mineralogical identification was carried out using X-ray powder diffraction (XRD) (Bruker D8 Advance diffractometer with Vantec Super Speed detector) and Raman spectroscopy (Renishaw InVia Raman spectrometer with a 785nm laser). Reflectance measurements of solid samples have been made using an Ocean Optics Jaz spectrometer and ISP-REF integrating sphere in 8° incident / total hemispherical reflection geometry. A summary of sample properties is presented in Table 2 and full details of the samples and their characterization, and the development of the F2-12 filter set may be found in [3].

The reflectance spectra of the Mars analogue samples along with simulated measurements from the centre and edge of the PanCam field of view and a cubic spline fitted to the data using the method outlined above are plotted in Fig 5. The data points which would be measured by PanCam assuming no wavelength shift are joined by straight lines to illustrate the data that would normally be obtained. Features of particular interest are shown inset and enlarged.

TABLE I. F2-12 FILTER SET AND SHIFTED CENTRE WAVELENGTHS

Filter No	**F2-12 centre wavelength (nm)**	
	Normal incidence	***17° incidence (1% shift)***
1	440	435.6
2	470	465.3
3	510	504.9
4	560	554.4
5	590	584.1
6	650	643.5
7	710	702.9
8	750	742.5
9	820	811.8
10	890	881.1
11	960	590.4
12	1000	990

TABLE II. MARS ANALOGUE SAMPLE PROPERTIES

Sample Name	Sample Properties		
	XRD	*Raman*	*Vis-Nir*
NAL_R	Alunite / Natroalunite	Hematite	Alunite
NBO	Jarosite	Jarosite	Jarosite

Further details of the samples and their characterization including XRD and Raman data, backscattered SEM images and EDS spot measurements may be found in [3].

It can be seen that in both cases features which would otherwise be missed are represented accurately by the fitted cubic spline. In particular for both samples the F2-12 data shows an almost straight line between 440 – 510nm whereas the cubic spline at least partially recreates the subtle shoulder in the original reflectance spectrum. For the sample NAL-R the cubic spline accurately recreates the change in gradient between 590 - 650nm and also more accurately represent the gradient between 750 - 890nm. For the NBO sample the cubic spline accurately recreates the reflectance spectrum between 710 - 750nm allowing the location of the characteristic peak of Jarosite to be accurately determined.

IV. FURTHER DEVELOPMENTS

The simulations presented assume that multispectral images are taken with a conventional filter wheel camera such as PanCam. However by designing a camera system with the intention of exploiting the wavelength shift it is possible to obtain much more spectral information. By inspection of Fig 3 it can be seen that the same angle of incidence and hence the same spectral shift will be obtained either side of the field of view. If the filter is deliberately mounted in front of the lens at an angle equal to half the field of view then a greater and asymmetric dispersion will be achieved across the field of view. The un-shifted filter wavelength will be obtained at one side of the field of view where the light rays pass through at normal incidence and progressively shorter wavelengths will be obtained as the angle of incidence increases towards the other side of the field of view as shown in Fig 6.

If the range of angles of incidence is doubled, the spectral range is more than doubled (see (1)). If the field of view is also increased then the spectral range can become comparable to the wavelength interval between the filters. In practice the useful range of angles of incidence of most interference filters is limited as the effective refractive index of the film stack is different for polarizations parallel and perpendicular to the plane of incidence. This causes progressively poorer out of band blocking due to polarization splitting as the angle of incidence is increased.

The VersaChrome range of filters recently developed by Semrock [10] are designed for use at angles of incidence up to 60˚ resulting in spectral shifts of up to 12% of their centre wavelength. With seven filters it is possible to completely cover the spectral range 340 – 800 nm. A filter wheel containing this set of filters, mounted at an angle of 30˚ in front of a lens with a 60˚ field of view as illustrated in Fig 6 would allow measurements to be taken at any wavelength over this range. A sequence of images taken with all of the filters whilst panning the camera by more than 60˚ would allow high spectral resolutions to be achieved.

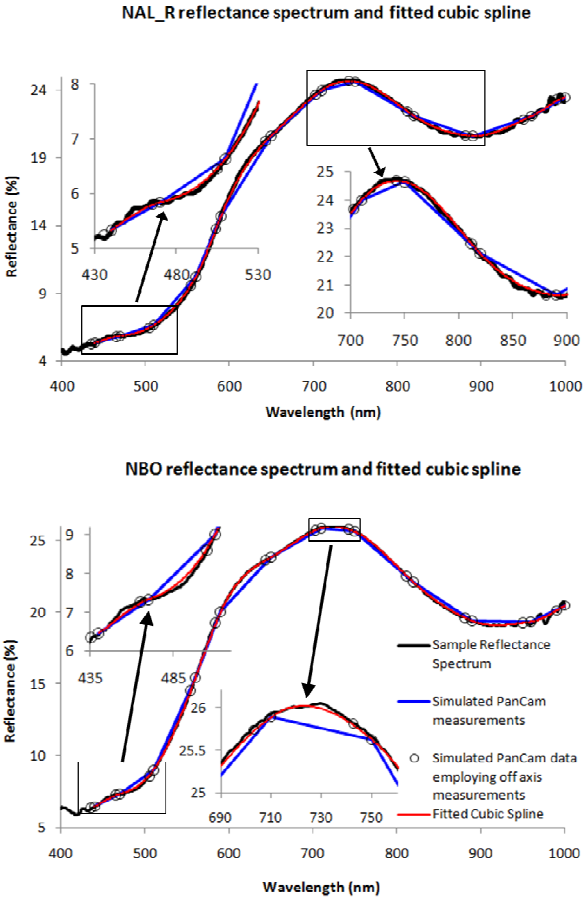

Figure 5. Mars analogue sample reflectance spectra showing simulated PanCam data points (right hand circle of each pair), data points which would be obtained at the edge of the field of view and a fitted cubic spline. The data points as measured by PanCam are linked by straight lines to show the features which would be missed. Insets show enlarged regions of interest from the spectra.

A prototype camera system is under development to test the effectiveness and practicalities of this method. A single VersaChrome filter covering the spectral range 550 – 620 nm (semrock part no TBP01-620/14-25x36) has been mounted in purpose made filter mount with a 30° tilt. This is mounted in front of a Starlight Xpress MX716 cooled CCD camera fitted

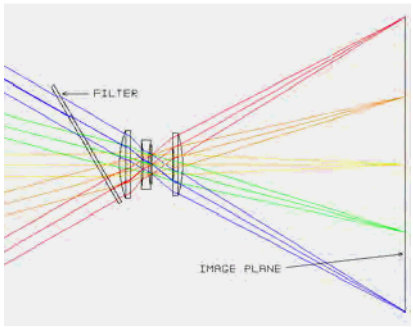

Figure 6. Ray diagram with a filter mounted tilted by 30˚in front of a Cook triplet lens with 60˚ field of view [7]. Showing how the angle of incidence of the light through the filter varies with image height.

with an Edmund optics Techspec u-video lens with a 6mm focal length (part no R58-842) giving a field of view of 56° horizontally and 66° diagonally. The filter is mounted so that the left hand side of the image is taken with 550nm light and the right with 620nm. This camera is at an early stage of development and much work still needs to be done on calibration and image processing algorithms before it can be used to generate hyperspectral images.

Preliminary tests and calibration measurements have been made with the camera by mounting it in front of a Labsphere integrating sphere. White light from a tungsten lamp was coupled into a Hilger & Watts D290 monochromator the output of which was directed into the integrating sphere. In this way the camera imaged the back wall of the integrating sphere which could be uniformly illuminated with any wavelength by adjusting the monochromator. The wavelength and relative intensity of the light in the integrating sphere was monitored with an Ocean Optics Jaz spectrometer. Dark frames were subtracted from the camera images and they were normalized to flat field images to remove intensity variations introduced by vignetting in the lens. A sequence of calibration images is presented in Fig 7 along with a color image taken through the tilted filter with a DSLR fitted with a wide angle lens to illustrate the variation in wavelength across the field of view.

It can be seen from Fig 7 that as the wavelength of the incident light is altered from 620 – 550nm, arcs with increasing radii move across the field of view demonstrating that different regions of the field of view are exposed to different wavelengths. The dispersion takes the form of arcs as the angle of incidence increases symmetrically either side of the centre in the vertical direction and progressively in the horizontal direction. The centre of the arcs is the point where the light passes through the filter at normal incidence.

CONCLUSIONS

The limitations on mass and power imposed on hardware used for planetary exploration has limited scientific cameras to multispectral capabilities with around 12 wavelengths. By exploiting properties inherent to interference filters it is possible to obtain additional spectral information with existing multispectral camera technology simply by imaging the same object at different points across the field of view of the camera. This additional information allows a cubic spline to be fitted through the measured data, providing a more accurate recreation of the original spectrum than is otherwise possible.

By designing a wide angle camera with the intention of exploiting the spectral shift obtained by tilting interference filters and making use of recent developments in filter technology it will be possible to develop a camera employing a small number of filters capable of obtaining full hyperspectral images by panning the camera. It is envisaged that such a camera could be used on future planetary exploration missions to obtain continuous high resolution reflectance spectra.

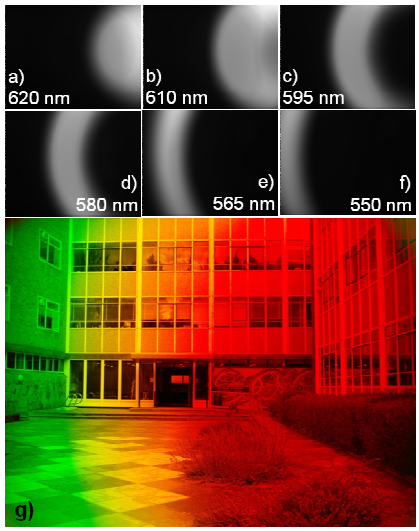

Figure 7. a – f) Calibration images from the prototype hyperspectral camera for different incident wavelengths. g) a colour image of the Institute of Maths and Physics at Aberystwyth university taken through the tilted filter with a DSLR to illustrate the dispersion.

ACKNOWLEDGEMENT

Support for this work was provided by the Centre for Advanced Functional Materials and Devices (CAFMaD), a HEFCW funded reconfiguration and collaboration project. Research leading to this work has been funded by the UK Space Agency, Grant No. ST/G003114/1, & Grant No. ST/I002758/1, & from the European Community's Seventh Framework Program (FP7/2007-2013), Grant Agreement No. 218814 (PRoVisG), and Grant Agreement No. 241523 (PRoViScout).

REFERENCES

[1] J. Vago, "ExoMars Science Management Plan," EXM-MS-PL-ESA-00002, 12 Feb 2010 2010.

[2] A. D. Griffiths, et al., "Context for the ESA ExoMars rover: the Panoramic Camera (PanCam) instrument," International Journal of Astrobiology, vol. 5, pp. 269-275, 2006.

[3] C. R. Cousins, et al., "Astrobiological Considerations for the Selection of the Geological Filters on the ExoMars PanCam Instrument," Astrobiology, vol. 10, pp. 933-51, 2010 Nov 2010.

[4] X. Baillard, et al., "Interference-filter-stabilized external-cavity diode lasers," Optics Communications, vol. 266, pp. 609-613, Oct 15 2006.

[5] A. D. Griffiths, et al., "The Beagle 2 stereo camera system," Planetary And Space Science, vol. 53, pp. 1466-1482, 2005.

[6] J. F. Bell, et al., "Mars Exploration Rover Athena Panoramic Camera (Pancam) investigation," Journal Of Geophysical Research-Planets, vol. 108, Nov 29 2003.

[7] G. H. Smith, Camera lenses from box camera to digital: SPIE Press, 2006.

[8] S. Pugh, L. Tyler, and D. Barnes, "Automatic Pointing and Image Capture (APIC) for ExoMars type mission," in The 10th International Symposium on Artificial Intelligence Robotics and Automation in Space, Japan, 2010.

[9] C. R. Cousins, et al., "Selection of the Geological Filters on the ExoMars PanCam Instrument." 42nd Lunar and Planetary Science Conference, 2011, Abstract #1826.

[10] T. Erdogan and L. Wang, "Semrock VersaChrome the first widely tunable thin-film optical filters," Semrock.